International Communications in Heat and Mass Transfer 179 (2026) 112259

Contents lists available at ScienceDirect

International Communications in Heat and Mass Transfer

journal homepage: www.elsevier.com/locate/ichmt

Thermal efficiency enhancement in battery thermal management systems by incorporating phase change materials in nano-encapsulated form into the base fluid

Maoqing Xie [a], Leigang Wang [b,*], Kexin Ding [a], Mahmut Taner [c], Soheil Salahshour [d,e,f,g,**], Aydin Secer [h]

[a] Hangzhou Polytechnic, Hangzhou, Zhejiang 311402, China
[b] School of Materials Science and Engineering, Jiangsu University, Zhenjiang, Jiangshu 212013, China
[c] Faculty of Engineering and Architecture, Istanbul Gelisim University, Istanbul, Türkiye
[d] Faculty of Engineering and Natural Sciences, Istanbul Okan University, Istanbul, Turkey
[e] Faculty of Engineering and Natural Sciences, Bahcesehir University, Istanbul, Turkey
[f] Research Center of Applied Mathematics, Khazar University, Baku, Azerbaijan
[g] Faculty of Science and Letters, Piri Reis University, Tuzla, Istanbul, Turkey
[h] Department of Computer Engineering, Biruni University, 340109 İstanbul, Turkey

ARTICLE INFO

Keywords:
Forced convection
Thermal management
Nano-encapsulated PCMs
Energy storage
Cooling batteries

ABSTRACT

The increasing variety of mechanisms and sources for energy extraction has drawn considerable attention to the long-term storage of energy. Phase change materials (PCMs) can retain heat for extended periods. This research presents a case study of lithium battery thermal management (BTM) via numerical simulation. We aim to store energy and enhance heat transfer by utilizing nano-encapsulated phase change materials (NEPCMs). We performed simulations of both steady and unsteady forced convection using C++ − based OpenFOAM solvers. The pimpleFOAM and simpleFOAM solvers have been improved to incorporate the effects of NEPCMs within the governing equations. The simulations demonstrate that, under both steady and unsteady conditions with high heat flux, the addition of NEPCM particles reduces the battery surface temperature. Specifically, integrating 5% nanoparticles into water results in a decrease in temperature of up to 2 K in steady-state simulations and up to 4 K in unsteady-state simulations. However, at elevated Reynolds numbers, the presence of nanoparticles diminishes pressure. Moreover, incorporating NEPCMs into water promotes a more uniform temperature distribution across the battery cell surface. In particular, adding 5% NEPCM to water resulted in a nearly 36% reduction in UT values.

1. Introduction

Alongside the importance of energy harvesting, storing energy is also crucial [1]. The imbalance between power generation and its consumption creates some issues and challenges for energy-related systems. During high-power and low-power consumption, the excess generated power should be wasted [2,3]. However, storing the extra generated power for later use is more economical and environmentally friendly. Therefore, batteries and thermal storage tanks are recommended by researchers and engineers [4]. A range of thermal storage tanks is used to capture thermal energy. Phase change materials (PCMs) are a proven technique for saving significant energy at relatively low temperatures [5,6]. Materials change their physical states at almost constant temperatures; for instance, ice melts at approximately $0^{\circ}C$ at atmospheric pressure and stores 334 kJ/kg of energy. The stored latent energy is released during the phase change [7]. Therefore, using PCMs in energy systems can improve a system's thermal performance. Singh and Sahoo [8] analyzed the hybrid cooling method of a battery by using conjugate heat transfer in CFD. They used a special nanoparticle shape in the PCM, also contributing to water. They also compared different PCMs and reported that using n-octadecane has the best thermal performance.

Afzal et al. [9] assessed the Li-ion battery pack cooling by using paraffin wax PCM. They demonstrated that adding Si—C nanoparticles

* Corresponding author at: School of Materials Science and Engineering, Jiangsu University, Zhenjiang, Jiangshu 212013, China
** Corresponding author at: Faculty of Engineering and Natural Sciences, Istanbul Okan University, Istanbul, Turkey.
E-mail addresses: wangleigang971061@126.com (L. Wang), soheil.salahshour1361@gmail.com (S. Salahshour).

https://doi.org/10.1016/j.icheatmasstransfer.2026.112259

Available online 12 August 2026

Nomenclatures

C_r	Heat capacity ratio of the nanofluid to the base fluid
C_p	Specific heat capacity $\left(J/_{kgK}\right)$
D	Diameter of the battery (m)
H	Enthalpy (J)
h_0	Standard enthalpy of formation $\left(J/_{kg}\right)$
k	Thermal conductivity $\left(W/_{mK}\right)$
l	Inlet diameter of the cooling channel (m)
L_{sf}	Latent heat capacity $(J/_{kg})$
p	Pressure (Pa)
P_{drop}	Pressure drop
Pr_w	Prandtl number
Re	Reynolds number
T	Temperature (K)
T_{Melt}	Temperature range of the Melting process (K)
T_{fusion}	Melting temperature (K)
$\overline{T}_{battery}$	Local-averaged temperature on the battery surface
U	Velocity in the x direction $\left(m/_{s}\right)$
U_T	Thermal uniformity factor
V	Velocity in y direction $\left(m/_{s}\right)$

Greek symbols

θ	Non-dimensional melting temperature
μ	Dynamics viscosity $\left(kg/_{ms}\right)$
ϑ	Kinematic viscosity $\left(m^2/_{s}\right)$
ρ	Density $\left(kg/_{m^3}\right)$

Subscripts

battery	Surface of the battery
c	Core
f	Fusion
n	NEPCM particles
nf	Nanofluid
l	Liquid phase
s	Shell

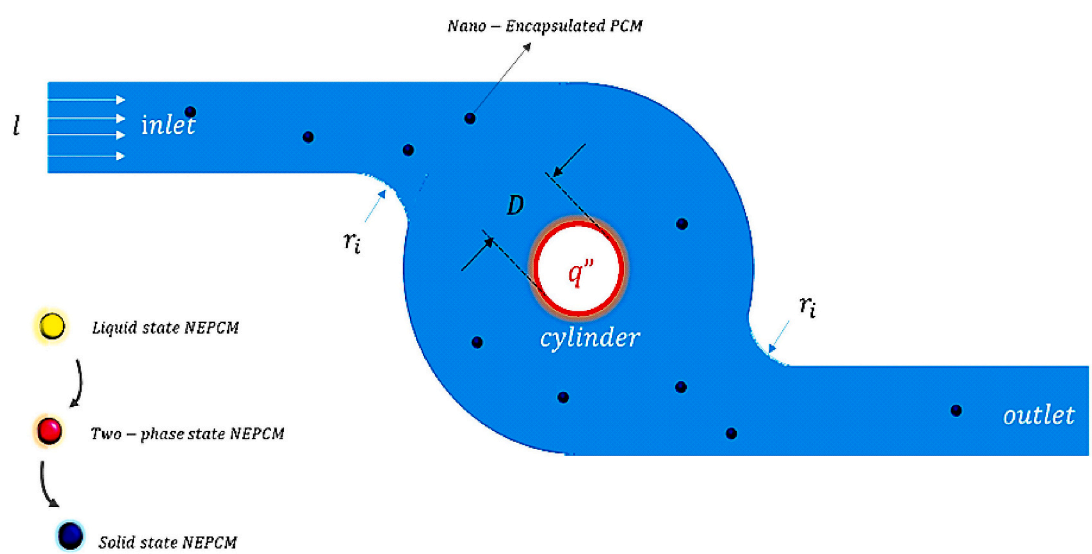

Fig. 1. The presentation of the studied case included a cooling channel, a battery, and NEPCMs.

can enhance cooling performance and also thermal uniformity inside the PCM. Several studies have designed and optimized thermal systems [10,11]. Despite the advantages of PCMs, several concerns and challenges exist [12]. PCMs are often implemented in containers, façades, tanks, and other similar applications [13]. A common drawback of these applications is the immobility of PCMs. PCMs are typically installed as a package and are not usually portable [14]. The researcher addresses this issue by encapsulating PCMs at the micro- and nanoscale.

In that way, nano-encapsulated PCMs (NEPCMs) or micro-encapsulated PCMs (MEPCMs) can be pumped and transported through pipes [15]. Nowadays, NEPCMs have received special interest in cooling systems and solar collectors. Tayebi et al. [16] numerically investigated the use of NEPCMs in electrohydrodynamic fluid flow in the presence of active heat sources in the steady-state condition. They reported that using 3% NEPCMs can improve heat transfer by 4.4%. Reddy and Sreedevi [17] studied a thermal storage system containing n–eicosane–based NEPCMs. They changed and analyzed different parameters related to NEPCMs and porous media. They proposed that in industrial applications, further modification of NEPCM parameters is necessary. A large part of NEPCM analysis is related to thermal energy storage systems [18,19]. Sadr et al. [20] modeled the mixed convection of Nonadecane-based NEPCMs within a water fluid in a cavity with a hot inner cylinder. They reported that adding NEPCMs to the base fluid can improve Nu_{ave}. Kazemi-Varnamkhasti [21] analyzed the presence of Nonadecane NEPCM in the cooling channel of a PEM fuel cell under forced convection. Their research revealed that adding 4% of nonadecane NEPCMs improves heat transfer rate by 20% and heat storage by 18%, respectively. Ho et al. [22] studied the effects of water-NEPCM nanocapsules in a heatsink cooling system experimentally. The NEPCM capsules contain eicosane in the core and formaldehyde for the shell. They reported that the heat transfer rate was improved by 70% with the addition of NEPCM. Fan et al. [23] studied an air-cooled lithium-ion battery module, and they concluded that using PCM is crucial to prevent an intense temperature gradient.

Table 1
Constant properties of the base fluid and NEPCMs at room temperature [38].

	$\rho\left(\frac{kg}{m^3}\right)$	$C_p\left(\frac{J}{kgK}\right)$	$\beta\times 10^{-5}\left(\frac{1}{K}\right)$	$k\left(\frac{W}{mK}\right)$	$\mu\left(\frac{kg}{ms}\right)$
Water	997	4182	2.9	0.62	800×10^{-6}
Core – nonadecane	720	2040	52	0.2	–
Shell – polyurethane	780	1320	18.2	0.02	–

Furthermore, there has been considerable interest in merging conventional battery cooling systems with PCM over the last few years. Extensive studies have investigated liquid-PCM thermal management systems [24]. However, few studies have been done regarding adding nano-encapsulated PCMs to the base fluid in the cooling channels [23]. Sutheesh et al. [25] simulated a multi-layer cooling system for a 18,650-30Q lithium-ion battery using Tetradecan-1-ol-based NEPCMs with different concentrations. They reported that adding 4% NEPCM can increase the convective heat transfer coefficient by 6.15 times compared with deionized water. Gu et al. [26] studied thermal management of Li-ion batteries using NEPCMs with paraffin and silica. They reported that adding NEPCMs to the pure oil reduced the mean temperature by up to 3.95 °C. In addition to limited studies on NEPCMs for battery cooling, numerous studies have demonstrated that the nonadecane core material in NEPCM can be highly effective at enhancing heat transfer in various systems. However, the effect of these materials in lithium-ion batteries has not been investigated. In the present study, a cylinder serving as a hot battery will be cooled using a NEPCM-water nanofluid. The presented battery thermal management system was simulated for both steady-state and unsteady conditions. The effects of heat flux, *Re* number, and the addition of nanoparticles to water are assessed. The primary objective of the current study is to reduce the battery's surface temperature. Therefore, in addition to velocity and pressure drop, temperature contours and diagrams are also presented.

2. Presentation of case study

Fig. 1 shows the battery cooling channel. The battery in the center of the channel is simulated as a hot cylinder. The inlet fluid receives heat from the hot cylinder and exits at the outlet. In Fig. 1, the ratios of l/D and r_i/D are 0.5 and 1/3. Where D = 18 mm [4]. Two types of working fluids have been evaluated in this study: pure water and a water-based NEPCM. The nano-encapsulated phase change materials (NEPCMs) begin to melt at 305 K. At temperatures below this value, NEPCMs are in the solid state, and at higher temperatures, they melt. The PCM is composed of n-nonadecane inside the nanoparticle core, and polyurethane is the capsule shell. n-Nonadecane is chosen as a core for melting within a temperature range suitable for its use in BTMS [27–36]. Furthermore, the Polyurethane shell has attracted the attention of engineers due to its high strength and low crystallinity [37].

The phase change materials melt at T_m and in the δT_m temperature range. The following equations express the enthalpy energy of phase change materials:

$$H = h + \Delta H \tag{1}$$

$$h = h_0 + \int_{T_0}^{T} C_p dT \tag{2}$$

$$\Delta H = \alpha\, L_{sf} \tag{3}$$

The total enthalpy values of the PCMs (H) consist of two terms, h and ΔH, which are known as sensible energy and latent energy, respectively. The sensible energy, as its name implies, appears as a change in temperature (ΔT), but latent energy appears in the phase-changing process at a constant temperature. In Eq. 2, h is specific enthalpy, h_0 is the standard enthalpy of formation, and C_p is the specific heat capacity. Also, in Eq. 3, the α parameter indicates the melting mass rate, and L_{sf} is the required energy for the phase change process. Eqs. 1–3 are generally applicable to phase change materials. For NEPCMs, these equations are modified [20], and the effects of latent energy changes are combined with sensible energy. Since the phase change occurs at a fixed temperature, these effects are applied to C_p values for NEPCM. Which is generally provided by the following equations:

$$C_{p,total} = C_p + \Delta C_P \tag{4}$$

$$\Delta C_P = \left\{\frac{\pi}{2}\left(\frac{L_{sf}}{\delta T_M} - C_{p\,c,l}\right)\left(\sin\pi\frac{T-\left(T_M - \delta T_M/2\right)}{\delta T_M}\right)\right\} \times \begin{cases} 0 \text{ if } T < T_f - \frac{\delta T_M}{2} \\ 1 \text{ if } T_M - \frac{\delta T_M}{2} < T < T_M + \frac{\delta T_M}{2} \\ 0 \text{ if } T < T_M + \frac{\delta T_M}{2} \end{cases} \tag{5}$$

In this study, $C_{p,total}$ is known as the C_p value of the core inside NEPCMs. In Eq. 4, ΔC_P is the value of heat that is saved in the phase change $\left(\Delta C_P \cong \frac{L_{sf}}{\delta T_M}\right)$. In Eq. 5, L_{sf} is the melting-solidification latent heat capacity, T_M is the solidification-melting temperature, also δT_M is the temperature range of the phase change. Where the value of $\delta T_M$is equal to 2.5 K [38]. Since NEPCMs themselves consist of a core and a shell, the C_p of nanoparticles is as follows [38]:

$$C_{p,n} = \frac{\left(C_{p,total} + \vartheta C_{p,s}\right)\rho_c\rho_s}{\left(\rho_s + \vartheta\rho_c\right)\rho_n} \tag{6}$$

In Eq. 6, ρ is the density. The subscripts c and s represent the core and shield. The ϑ is the volume ratio of core to shell. Finally, according to the above explanations, in addition to previous studies, the thermo-physical properties of water fluid and NEPCM are as follows [21]:

$$\rho_{nf} = (1-\varphi)\rho_{bf} + \varphi\rho_n \tag{7}$$

$$C_{P,nf} = \frac{(1-\varphi)\rho_f C_{P,b\,f} + \varphi\rho_n C_{P,n}}{\rho_{nf}} \tag{8}$$

In the above equation, φ is the concentration of nanoparticles, which is equal to 5% in this paper. Other thermophysical properties are demonstrated in Table 1.

The dynamic viscosity and thermal conductivity of the nanofluid are obtained according to the experimental results of Qiu and Li [39]:

$$k_{nf} = k_{bf}\sum_{i=0}^{i=5} a_i\,\varphi^i \tag{9}$$

$$\mu_{nf} = \mu_{bf}\left[1 + \frac{\varphi}{8} + \left(6\times 10^{-4}\varphi^2\right)\right] \tag{10}$$

where $a_0 = 1, a_1 = -0.3925, a_2 = 0.7141, a_3 = -0.4177, a_4 = 0.1055,$ and $a_5 = -0.0098$ [39].

The steady-state forms of the mass, momentum, and temperature conservation are presented below. The simulation is considered to be incompressible and two-dimensional. Additionally, the effects of gravity are often overlooked [40,41].

$$Mass\ Conservation: \frac{\partial u}{\partial x} + \frac{\partial v}{\partial y} = 0 \tag{11}$$

Table 2
Presentation of the post-processing parameters.

Symbol	Equation	Definition
P_{drop} (−)	$\frac{\Delta P}{\frac{1}{2}\rho U_{ave}^2}$	Pressure drop
$\overline{T}_{battery}$ (K)	$\frac{1}{A_b}\int_0^{2\pi} T\, r\, d\theta$	Local-averaged temperature on the battery surface
U_T (K)	$U_T = \frac{\int \lvert T - \overline{T}_{battery}\rvert\, dA}{A_b}$	Temperature uniformity on the battery surface
$\overline{\Delta T}_{battery}(K)$	$\overline{T}\rvert_{water} - \overline{T}\rvert_{water-NEPCM}$	Temperature drop in the presence of NEPCM particles

Table 3
Average Nusselt number of water- Al_2O_3 nanofluid for different Rayleigh numbers (Ra) of the current study, experimental study of Ho et al. [43], and numerical simulation of Sheikhzadeh et al. [44].

Ra	Experimental data [43]	CFD simulation of [44]	Present study	Error
7.6×10^5	7.69	8.24	8.49	10.4%
1.93×10^6	10.35	10.54	11.23	8.5%
3.33×10^6	12.04	12.09	12.86	6.8%

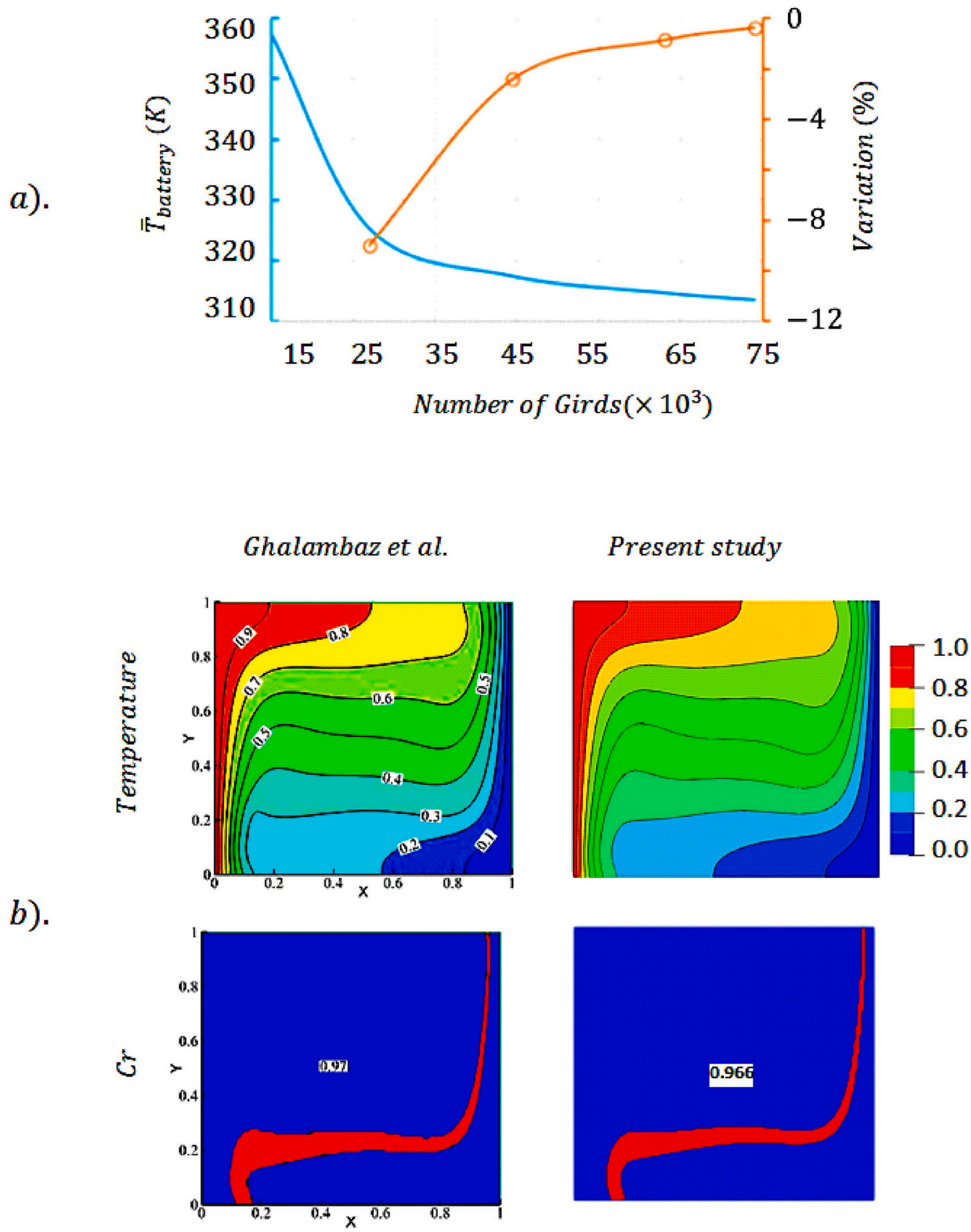

Fig. 2. a) Grid study of temperature variation vs. mesh numbers and b) Comparison of temperature and Cr contours for the current study and Ghalambaz et al. [42] for Ste $= 0.313$, Ra $= 10^5$, Pr $= 6.2$, and $\theta_f = 0.3$.

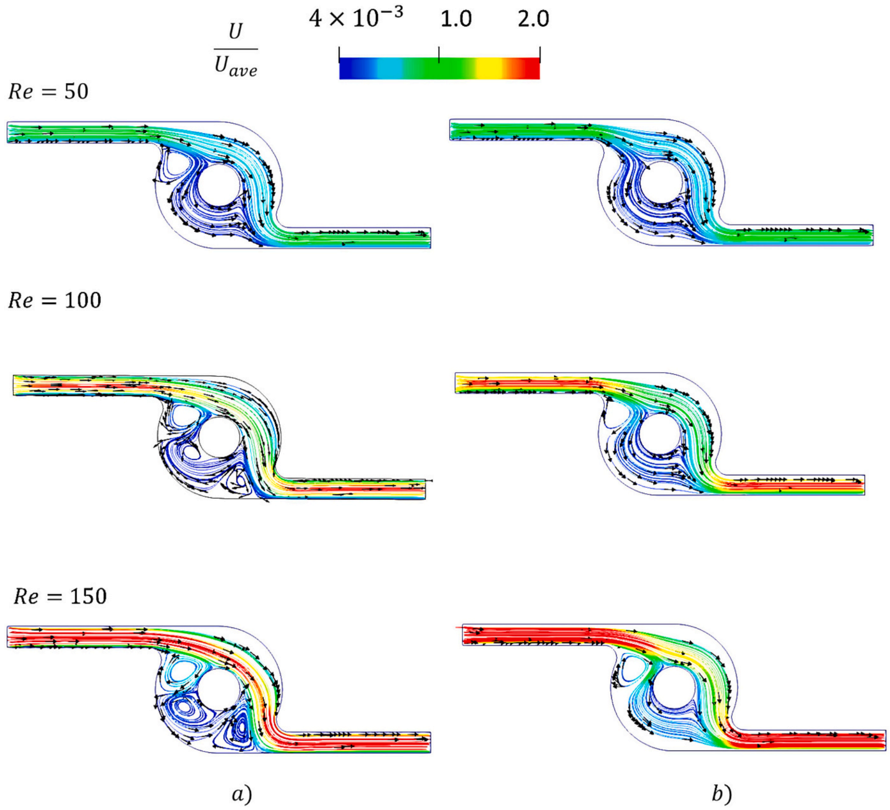

Fig. 3. Streamlines and non-dimensional velocity distribution at different Reynolds numbers in q" = 600 ($\frac{W}{m^2}$) for a). Pure water and b) Water-NEPCM.

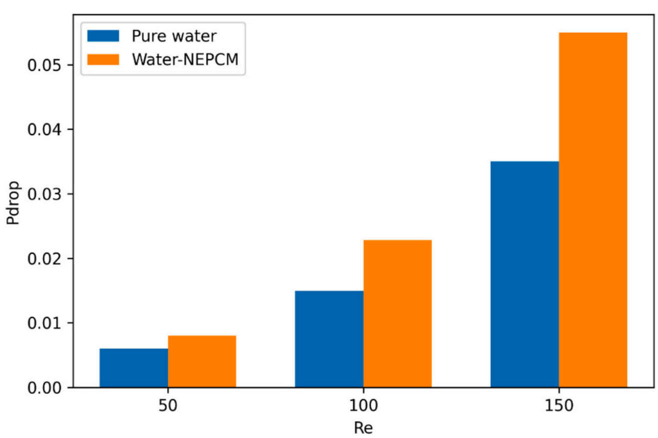

Fig. 4. Non-dimensional pressure drop at different Reynolds numbers in q" = 600 ($\frac{W}{m^2}$) for pure water and water-NEPCM.

$$Momentum\ in\ x-direction:\rho_{nf}\left(u\frac{\partial u}{\partial x}+v\frac{\partial u}{\partial y}\right)=-\frac{\partial P}{\partial x}+\mu_{nf}\left(\frac{\partial^2 u}{\partial x^2}+\frac{\partial^2 u}{\partial y^2}\right) \tag{12}$$

$$Momentum\ in\ y-direction:\rho_{nf}\left(u\frac{\partial v}{\partial x}+v\frac{\partial v}{\partial y}\right)=-\frac{\partial P}{\partial y}+\mu_{nf}\left(\frac{\partial^2 v}{\partial x^2}+\frac{\partial^2 v}{\partial y^2}\right) \tag{13}$$

$$Energy\ Conservatin:\left(u\frac{\partial}{\partial x}\left((\rho C_P)_{nf}T\right)+v\frac{\partial}{\partial y}\left((\rho C_P)_{nf}T\right)\right)=k_{nf}\left(\frac{\partial^2 T}{\partial x^2}+\frac{\partial^2 T}{\partial y^2}\right) \tag{14}$$

where u.v,p, and T are the velocity components in the x and y directions, the pressure field, and the temperature, respectively. μ_{nf}, k_{nf} and ρ_{nf} are the dynamic viscosity, thermal conductivity, and density of the nanofluid. A stream with a uniform velocity U_{ave} enters the channel from the input (Fig. 1) at a constant temperature of $T = 300$ K. The channel has insulated walls, and a non-slip velocity condition applies on the channel boundaries. The surface of the battery (the internal hot cylinder) experiences a constant heat flux in steady-state simulations and a time-varying heat flux in unsteady simulations. The velocity boundary condition on the cylinder is zero. At the outlet, a gradient null condition applies to both temperature and velocity, and the output pressure equals the atmospheric pressure. The important analysis parameters are presented in Table 2**.** Furthermore, a summary of the information and parameters used is provided in the appendix.

3. Grid study, solution method, and validation

The triangular mesh of the geometry shown in Fig. 1 is generated using Gambit 2.4.6. The fluid domain was discretized using an unstructured triangular mesh. Boundary-layer elements with a growth ratio of 1.1 were generated near walls to capture the thermal and hydrodynamic boundary layers accurately. Mesh quality was assessed using OpenFOAM's *checkMesh* utility. The maximum skewness remained below 1, while the maximum non-orthogonality was below 40, both of which satisfy the recommended criteria for accurate and stable CFD simulations. The sensitivity of the average temperature of the battery surface ($\overline{T}_{battery}$) on the mesh number is shown in Fig. 2**-a**. By refining the grid up to 63,000, the change of $\overline{T}_{battery}$ is remarkable. However, after this grid, the variation is almost 0.5%. This demonstrates the data's independence from the grid. Furthermore, a fixed Courant number is used for unsteady-state simulations. In this study, the Courant number is 0.2, and values below 0.2 do not significantly affect the data.

The SIMPLE and PIMPLE algorithms are also implemented to

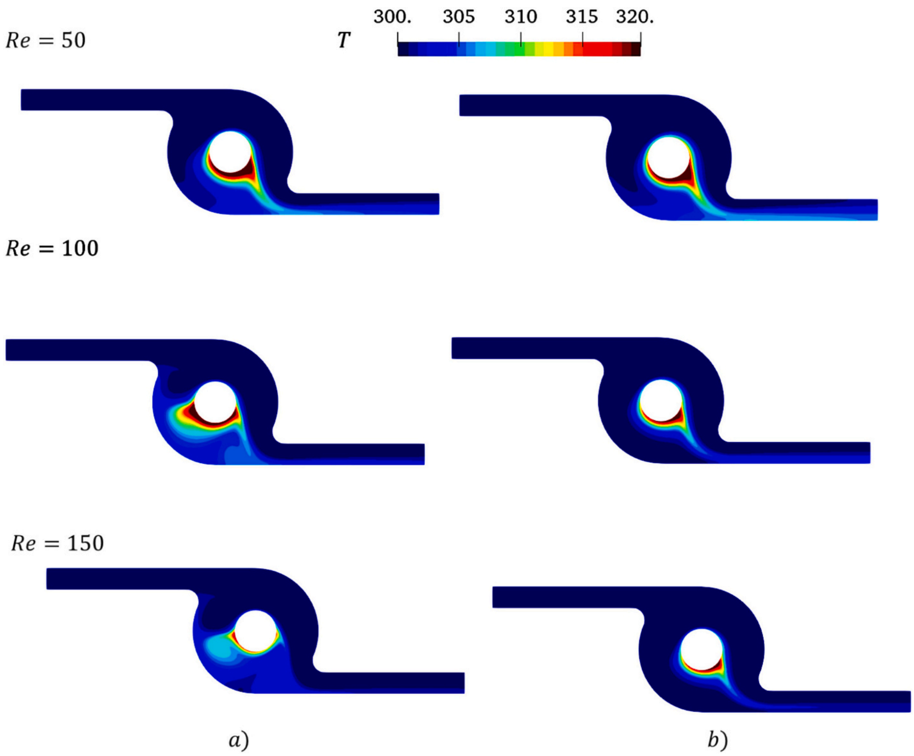

Fig. 5. Temperature distribution (K) at different Reynolds numbers in q” = 600 ($\frac{W}{m^2}$) for a). Pure water and b) Water-NEPCM.

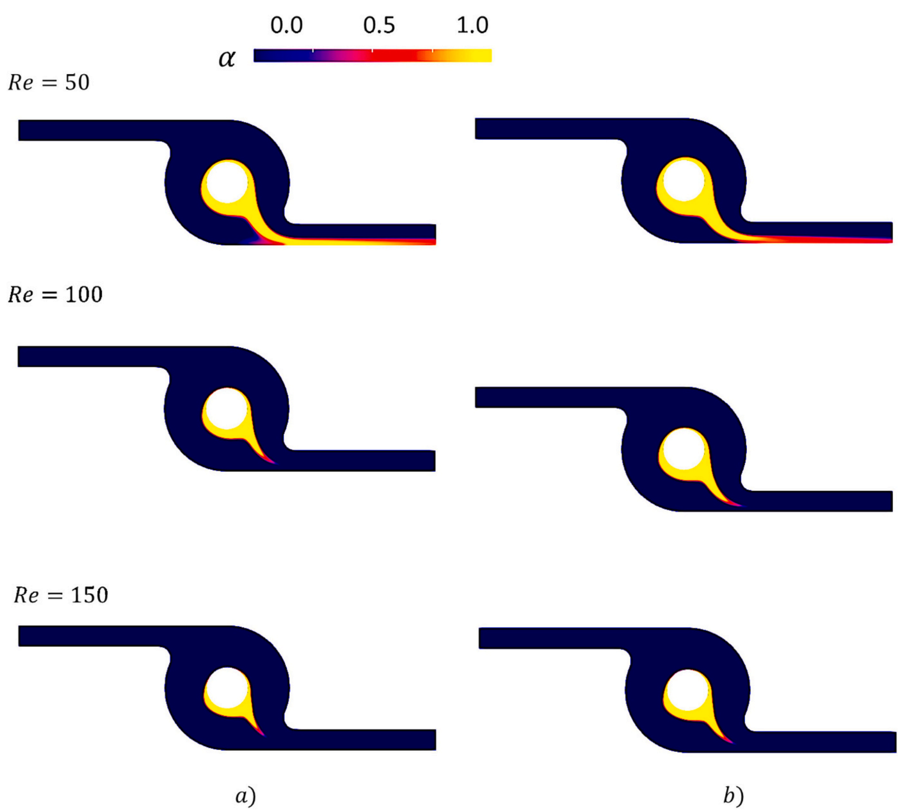

Fig. 6. Melting zone (α = 0 is solid and α = 1 is liquid state) at different Reynolds numbers for water-NEPCM nanofluid a). q” = 600 ($\frac{W}{m^2}$) and b). q” = 750 ($\frac{W}{m^2}$).

establish the link between the velocity and pressure fields in both steady and unsteady conditions. The 2nd-order upwind scheme is employed for the advection terms, while the 2nd-order central scheme is used for the diffusion terms. The values of relaxation factors for the fields of temperature, pressure, and velocity are 0.3, 0.7, and 0.7, respectively. Additionally, to verify our simulation, we reproduced the CFD results for nano-encapsulated PCMs presented by Ghalambaz et al. [42]. As shown in Fig. 2b, the data have acceptable accuracy.

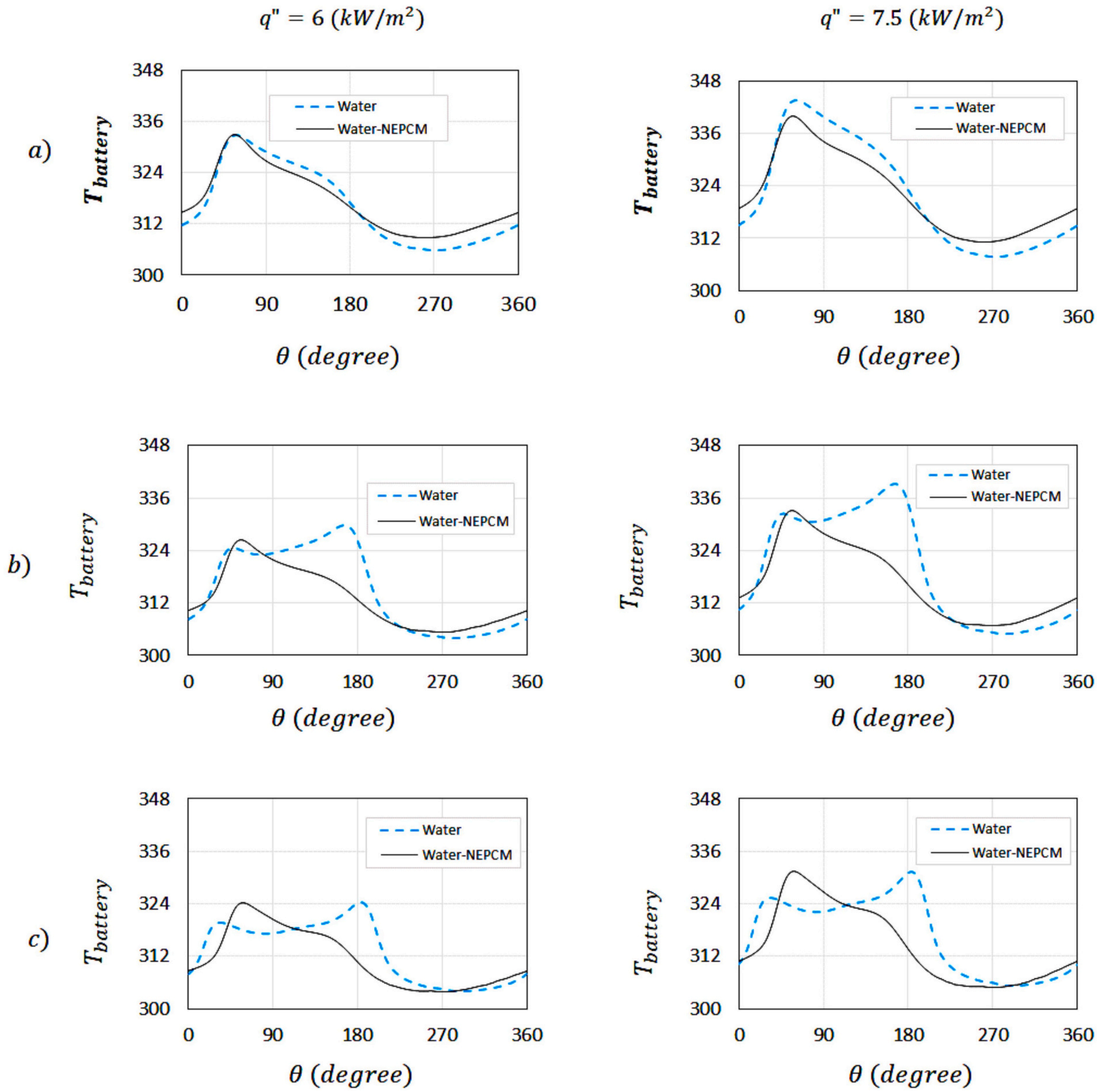

Fig. 7. Local temperature distribution at the battery surface (K) for different heat fluxes: a) $Re = 50$, b) $Re = 100$, and c). $Re = 150$. ($\theta = 0$ is located on the right side of the cylinder and increases in a clockwise direction).

Furthermore, to validate the numerical results against experimental data, the Nusselt number data reported by Ho et al. [43] were used. Ho et al. experimentally investigated the heat transfer of water and an Al_2O_3 nanofluid with a nanoparticle concentration of 0.01% at different Rayleigh numbers (corresponding to varying wall temperature differences). In addition, the present results were compared with the CFD simulations reported by Shekhzadeh et al. [44]. The comparisons are presented in Table 3. The error values were calculated based on the deviation of the present results from the experimental data. Overall, the results are well matched.

4. Results and discussion

In this part, we will analyze our simulated data. First, we will evaluate the impact of NEPCMs on flow patterns and pressure drop. Then, by establishing a significant relationship between velocity and energy performance, the effects of these nanoparticles under different conditions on fluid and battery surface temperatures will be studied.

4.1. Effects of NEPCM presence on flow and pressure parameters in constant heat fluxes

The velocity distribution results are presented in Fig. 3 at a constant heat flux. The purpose of this figure is to analyze the effects of the working fluid and the Reynolds number. We will first examine the effects of the inlet flow (represented by the Reynolds number) separately for each fluid, then examine the impact of the working fluid material. For pure water, in Fig. 3-**a**, in $Re = 50$, part of the fluid, when entering the circular channel, separates from the mainstream, and we see the production of a vortex, which we call vortex number 1. Additionally, at this Reynolds number, the fluid velocity is low. With increasing Reynolds number or increasing the inlet flow to the system, the number of created vortices increases (Fig. 3-**a** for $Re = 100$ and $Re = 150$). The fluid flow produces a new vortex as it leaves the circular chamber; after passing through the hot body, it is referred to as vortex 3. The middle vortex, referred to as vortex 2, is caused by the presence of vortex 3, which blocks the flow of fluid from beneath the hot cylinder. The story is a little different for nanofluids. In $Re = 50$, vortex number 1 is so small

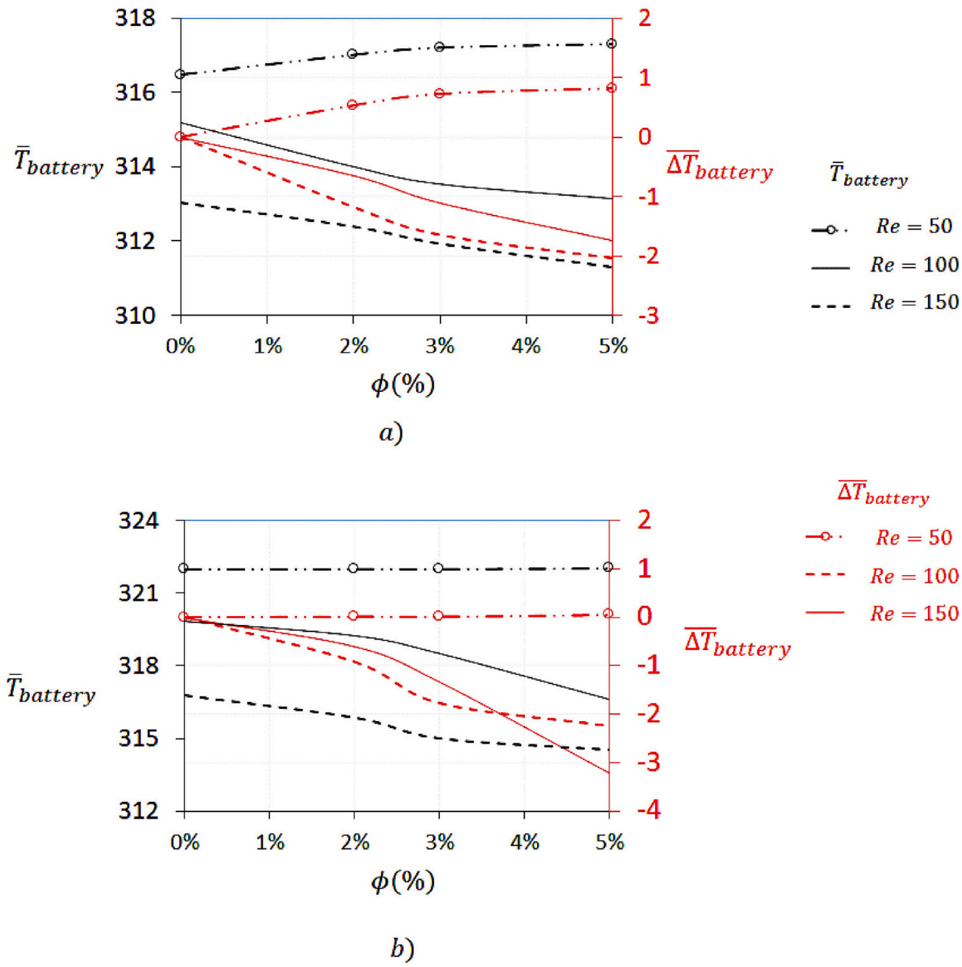

Fig. 8. The local average surface temperature of the battery (K) and temperature variation by adding NEPCM (K) for different concentrations of nanoparticles and *Re* numbers in a). q" = 600 ($\frac{W}{m^2}$) and b). q" = 750 ($\frac{W}{m^2}$).

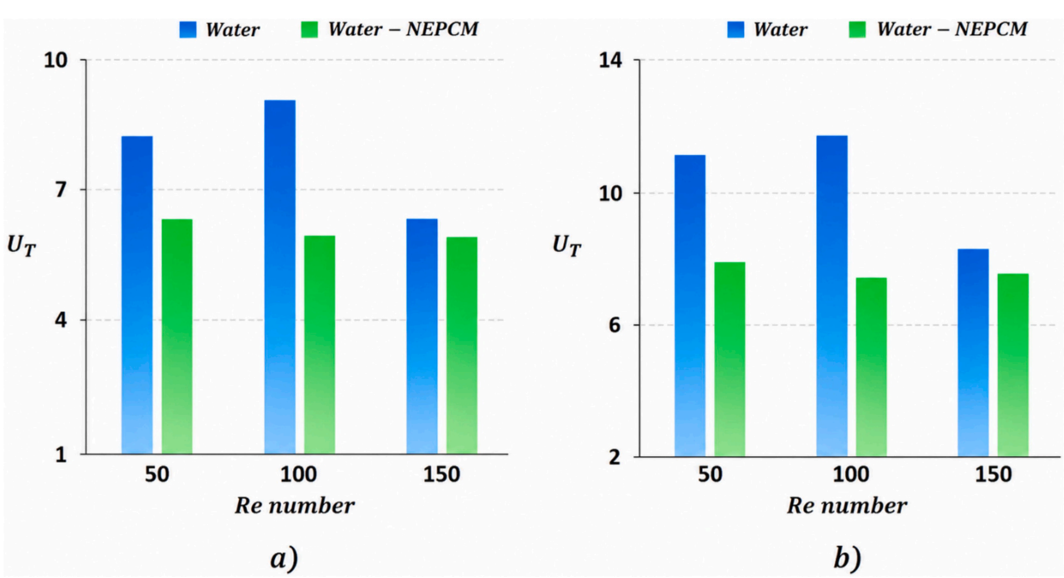

Fig. 9. U_T values (K) for different working fluids and *Re* numbers in a). q" = 600 ($\frac{W}{m^2}$) and b). q" = 750 ($\frac{W}{m^2}$).

that it has a velocity close to zero and is not visible, and with the increase of Reynolds number, there is no sign of vortex numbers 2 and 3. In *Re* = 150 it is observed that in the areas of vortex numbers 2 and 3, the fluid velocity for the water is lower than NEPCM.

Furthermore, the fluid flow around the hot cylinder for nanofluids is more uniform than in pure water. It is known that using nanoparticles increases water's viscosity. Flowing fluid in the channel becomes more difficult, which is why vortices No. 2 and 3 have not been created at high

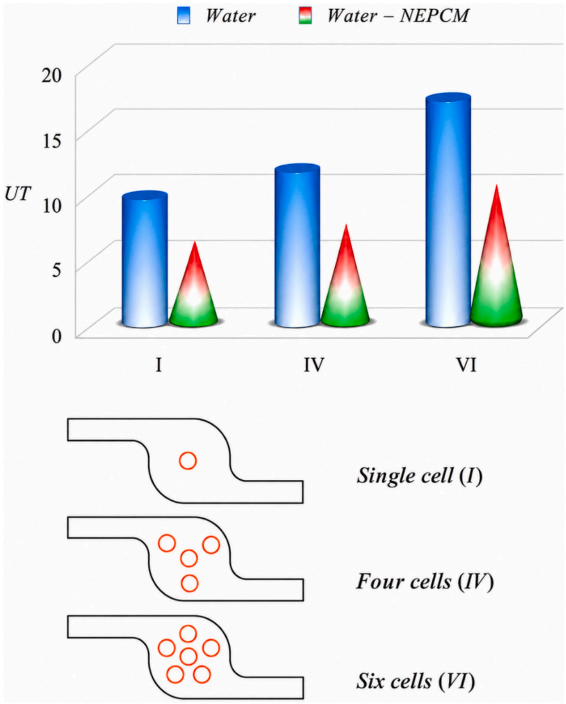

Fig. 10. U_T values (K) for different working fluids and battery cells in q" = 750 $(\frac{W}{m^2})$ and $Re = 100$.

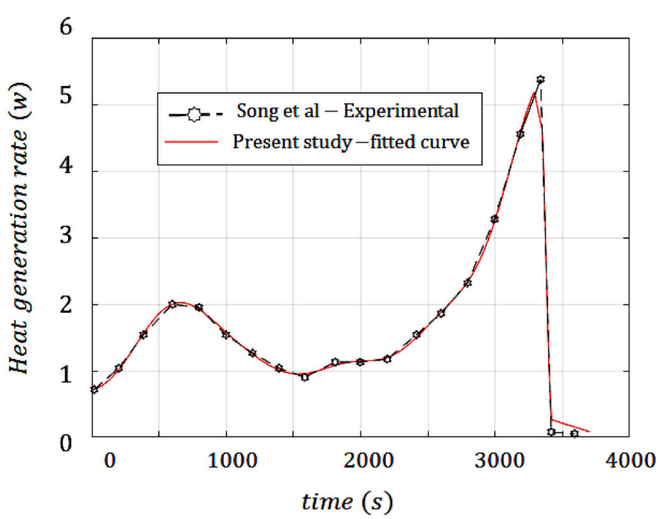

Fig. 11. The comparison of the fitted curve of heat generation rate (W) based on experimental data of Song et al. [45] during 1 °C discharging.

Reynolds numbers. To better illustrate the issue, the pressure drop diagram is presented in Fig. 4.

As shown in Fig. 4, the presence of nanoparticles in water caused a pressure drop in the cooling channel. Increasing the inlet flow velocity has also exacerbated this pressure drop. The physical reason for this phenomenon is that the nanoparticles in the base fluid create additional shear stress between the fluid layers, preventing the fluid from passing through, and the liquid molecules must carry these particles with them. At a high Reynolds number, nanofluid pressure drop values increased by up to 94% compared to water. This phenomenon is one of the disadvantages of having nanoparticles in the base fluid. Although nanoparticles enhance heat transfer and the system's thermal performance, the effects are presented in the next section.

4.2. Effects of NEPCM presence on thermal performance in constant heat fluxes

The temperature distribution within the domain for the heat flux of 600 $(\frac{W}{m^2})$ is shown in Fig. 5. For pure water (Fig. 5a), the temperature is low in the part of the hot cylinder where the fluid flow has directly impacted. Still, in the back of the hot cylinder, where the fluid has less contact with the cylinder, the temperature has increased. Additionally, the upper section of the hot cylinder has a lower temperature because its upper part has a higher velocity in its vicinity (Fig. 3). As the Reynolds number increases in pure water, the area of maximum temperature shifts. In the case of the three vortices (Fig. 3-**a** for $Re = 100$ and $Re = 150$), the highest temperature occurs in vortex area 2 because the vortex is relatively slow. At low velocities, the convective mechanism is low. Also, the fluid's temperature rises. However, the regions of maximum nanofluid temperature are the same at both Reynolds numbers. Also, the maximum temperature is almost the same for both working fluids. The temperature distribution on the hot cylinder will be evaluated in the following sections; however, we will first examine the melting zone of NEPCM throughout the domain.

The contours of the melting zones are shown in Fig. 6. According to this figure, there is a close relationship between the temperature distribution and the melting zone. At approximately 306 K, the core of NEPCMs begins to melt. At higher temperatures, the material inside the nanocapsules is liquid, and at lower temperatures, it is solid. As the Reynolds number increases, the melting zone becomes smaller because the strong convection offsets the increase in fluid temperature. As a result, the nanocapsules did not receive enough energy to melt. Additionally, increasing the heat flux has expanded the melting zone by transferring more heat to the fluid, providing more heat than required for melting within the NEPCMs. The effects of melting on the internal cylinder temperature are shown in Fig. 7.

The local temperature distribution is shown in Fig. 7. Comparing the graphs, it can be seen that pure water shows two temperature maxima, whereas adding NEPCMs results in a single maximum. This is due to the effects of adding NEPCMs on the viscosity and fluid density. These were analyzed in detail in Figs. 3 and 4. The second interesting point about the battery cell's temperature profile is the maximum temperature. If the nanocapsules melt and the melting zone is larger (due to high heat flux and low Reynolds numbers), the presence of nanocapsules reduces the maximum battery temperature. As shown in Fig. 6, this is due to the energy required to melt the phase change material. Since the phase change is a constant-temperature process, the nanofluid can absorb a significant amount of energy at a fixed temperature. This prevents the battery temperature from rising. As the heat flux increases, the battery surface temperature rises, a phenomenon observed in both fluids. Additionally, increasing the Re number enhances the system's cooling. Because the convective heat transfer coefficient is directly related to the Re number, increasing the Reynolds number increases the heat transfer coefficient, thereby preventing the battery surface temperature from rising.

The diagram of the local average of $T_{battery}$ and variation of $T_{battery}$ by adding nanoparticles ($\overline{\Delta T}_{battery} = \overline{T}|_{water} - \overline{T}|_{water-NEPCM}$) are shown in Fig. 8 for different concentrations of NEPCMs. In this figure, it can be seen that in almost all conditions, the presence of nanoparticles has reduced the battery surface temperature. However, at the lower Reynolds numbers, the nanoparticles did not perform very well. The reason is that adding nanoparticles to the base fluid increases viscosity and, consequently, reduces convective heat transfer, resulting in less heat transfer from the battery surface. This causes its temperature to rise.

On the other hand, increasing the nanoparticle volume fraction further decreases the cell surface temperature. The most significant temperature reduction is associated with a volume fraction of 5%. The reason is that by adding NEPCMS, the amount of $C_{p,nf}$ increases, which also appears in Eq. 8.

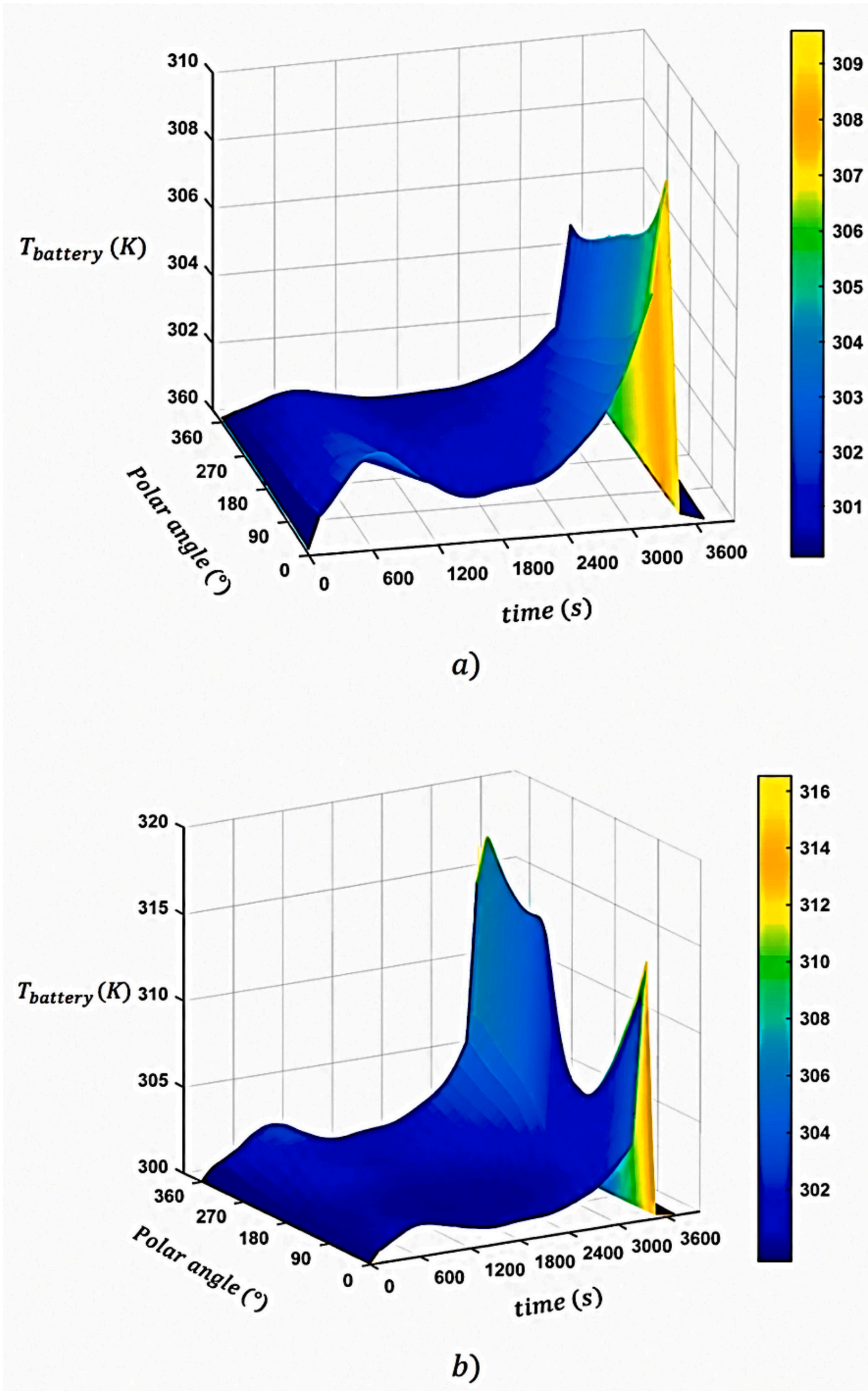

Fig. 12. Local and temporal temperature distribution at battery surface (K) for a). pure water and b). water-NEPCM.

To check the temperature uniformity on the surface, the U_T is defined. U_T values for different *Re* numbers and heat fluxes are presented in Fig. 9. Based on the definition of the U_T Parameter in Table 2: values close to zero indicate a more uniform distribution of temperature. Based on U_T, it can be seen that adding nanoparticles to water improves surface temperature uniformity on the battery. But with the increase of the *Re* number, the values of U_T For pure water and NEPCM-water, the values are nearly identical. At higher Re numbers, the increase in cell-surface temperature is also prevented by increasing the heat transfer coefficient. Since the rise in the heat flux has increased the maximum value of the $T_{battery}$ (Fig. 7), the U_T Values increase at high heat flux values. In the best case ($q^{''} = 750 \left(\frac{\mathrm{W}}{\mathrm{m}^2}\right)$ and $Re = 100$), by adding NEPCM to water U_T Values have decreased by almost 36%. In Fig. 10, the values of U_T For different compositions and numbers of battery cells, the corresponding values are given. By adding more battery cells, the value of U_T increases, because cold fluid does not completely cover the cylinder. This behavior of U_T is more obvious in the fluid. Increasing the number of battery cells strengthens the effect of nanocapsules because

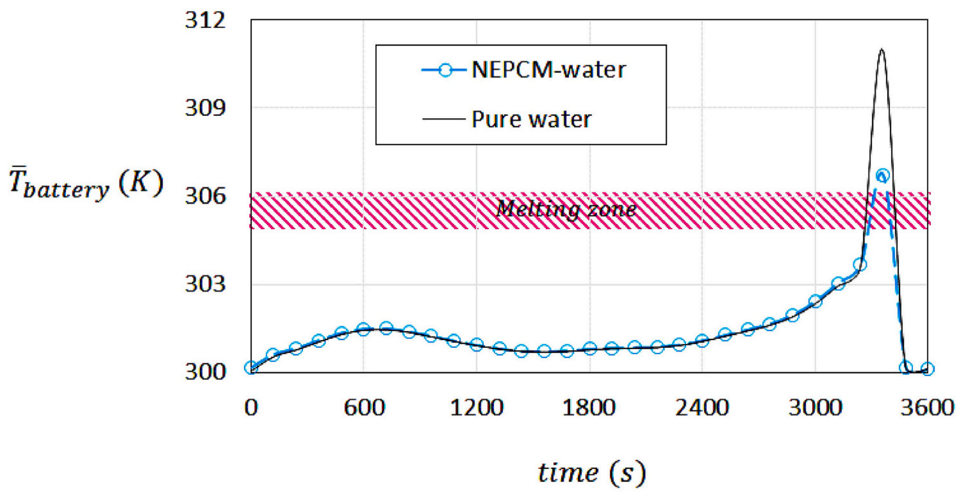

Fig. 13. The local average surface temperature of the battery over different time intervals.

more PCM is melted.

4.3. Effects of NEPCM presence on thermal performance in the time-varying heat flux

Here, we want to analyze the thermal performance of a single lithium-ion cell under transient conditions. Fig. 11 shows the energy production rate at 25 °C during discharge. To enhance simulation accuracy, the Fourier series curve-fitting method is employed to capture the experimental data of Song et al. [45].

A graph of battery surface temperature over time is presented in Fig. 12. In this study, the Reynolds number is constant at 50, and the nanoparticle volume fraction is 5%. It can be observed that using pure water increases the battery's temperature. Another noteworthy point is the shape of the temperature distribution diagram for these two fluids. The use of NEPCM nanocapsules shifts the maximum temperature. This phenomenon was also observed in steady-state conditions. In addition, for the highest temperature in both fluids in Fig. 11, the trend of the obtained thermal distribution diagram is close to the steady-state distribution.

To more closely examine the effects of NEPCMs under unsteady-state conditions, the average battery surface temperature at different times is presented in Fig. 13. As is known, when the production heat flux is low, the use of nanoparticles does not help much in cooling, but with the increase of the production flux and the melting of materials inside the nanocapsules, $\overline{T}_{battery}$ In the melting range, the temperature drops by almost $4^{\circ}C$. The melting zone of nanocapsules is highlighted in red. When the $T_{battery}$ As the volume fraction reaches the melting point, pure water raises the battery's temperature. Still, the presence of NEPCMs in the water causes these particles to store energy as latent heat, which, in turn, cools the battery surface further, lowering the water temperature.

5. Conclusion

In this study, the unsteady and steady-state battery thermal management systems under different conditions are investigated. The battery is considered a hot cylinder in the simulation to observe the effects of adding nano-encapsulated phase change material (NEPCMs). Additionally, the impact of the inlet flow Reynolds number and the heat flux generated by the battery has been analyzed. The following results can be presented:

- Using NEPCM nanoparticles increases viscosity and increases pressure drop. This reduces the number of vortices behind the hot cylinder.
- Increasing the concentration of NEPCMs lowers the cell's maximum temperature. Also, adding nanoparticles reduces the number of points with the maximum temperature.
- The presence of nanoparticles enhances surface temperature uniformity. These effects are more pronounced in high Reynolds numbers. The presence of NEPCM nanoparticles is also not recommended in low-Reynolds-number and low-heat-flux conditions.
- At high heat flux, the PCM materials melt and $\overline{T}_{battery}$ in the melting range, it drops by almost $4^{\circ}C$.
- By adding NEPCM to water U_T values reduce by up to 36%.
- At a high Reynolds number, nanofluid pressure drop values increased by up to 94% compared to water.

Despite the innovation, efforts, and convincing results, the present work has some disadvantages and limitations that should be addressed in future work. The biggest disadvantage of this work is the lack of laboratory data and the absence of prototype construction. Also, economic and environmental aspects of the problem are important. The authors also suggest that advanced modeling should be performed, including three-dimensional simulations and various channel and battery arrangements.

CRediT authorship contribution statement

Maoqing Xie: Writing – review & editing, Writing – original draft, Software, Resources, Investigation, Funding acquisition, Formal analysis, Data curation, Conceptualization. **Leigang Wang:** Writing – review & editing, Writing – original draft, Software, Resources, Investigation, Funding acquisition, Formal analysis, Data curation, Conceptualization. **Kexin Ding:** Writing – review & editing, Writing – original draft, Software, Resources, Investigation, Funding acquisition, Formal analysis, Data curation, Conceptualization. **Mahmut Taner:** Writing – review & editing, Writing – original draft, Software, Resources, Investigation, Funding acquisition, Formal analysis, Data curation, Conceptualization. **Soheil Salahshour:** Writing – review & editing, Writing – original draft, Software, Resources, Investigation, Funding acquisition, Formal analysis, Data curation, Conceptualization. **Aydin Secer:** Writing – review & editing, Writing – original draft, Software, Resources, Investigation, Funding acquisition, Formal analysis, Data curation, Conceptualization.

Declaration of competing interest

The authors whose names are listed immediately below certify that they have NO affiliations with or involvement in any organization or entity with any financial interest (such as honoraria; educational grants;

participation in speakers' bureaus; membership, employment, consultancies, stock ownership, or other equity interest; and expert testimony or patent-licensing arrangements), or non-financial interest (such as personal or professional relationships, affiliations, knowledge or beliefs) in the subject matter or materials discussed in this manuscript. Also, the authors whose names are listed immediately below report the following details of affiliation or involvement in an organization or entity with a financial or non-financial interest in the subject matter or materials discussed in this manuscript. Please specify the nature of the conflict on a separate sheet of paper if the space below is inadequate.

Acknowledgements

2025 Planning Project of the China Vocational Education Association (Grant No. ZJS2025YB102).

Appendix A. A summary of the information and parameters used is provided below

Parameter	Value / Range	Unit / Description	Clarification / Notes
Inlet Velocity (u_in)	Not directly stated, implied via *Re*	m/s	*Re* = 50, 100, 150. Calculated from *Re* = ρuD/μ.
Inlet Temperature	300	K	Uniform at channel inlet.
Wall Temperature	–	–	Insulated channel walls (adiabatic).
Battery Surface Boundary	Constant heat flux	600 or 750 W/m^2	Steady-state simulations; time-varying in transient.
Geometry	D_cylinder = 0.5, D_channel = 1/3	Non-dimensional	Used for scaling.
Reynolds Number (*Re*)	50, 100, 150	Non-dimensional	Computed using *Re* = ρuD/μ.
PCM Melting Temperature	~305–306	K	Phase change temperature.
Volume Fraction of NEPCM	0–5%	%	5% gives the maximum thermal improvement.
Latent Heat of PCM (Lf)	Symbolic only	J/kg	Used in enthalpy modeling.
Thermal Conductivity (k)	Water: 0.62, NEPCM core: 0.2	W/m·K	From Table 1.
Specific Heat Capacity (Cp)	Water: 4180, NEPCM core: 2040	J/kg·K	Thermal modeling values.
Dynamic Viscosity (μ)	Water: 0.001	Pa·s	NEPCM increases viscosity.
Density (ρ)	Water: 996, NEPCM core: 720	kg/m^3	From Table 1.
Non-Dimensional Pressure Drop	Up to +94% with NEPCM	Relative increase	Higher viscosity causes this.
Temperature Drop with NEPCM	Up to 4 K (unsteady), 2 K (steady)	K	Compared to pure water.
Temperature Uniformity Index (σT)	Reduced by 36%	Dimensionless	More even surface temperature.
Time-Varying Heat Flux	Fourier fitted from Song et al.	W	Used in unsteady analysis.
Governing Equations	Navier-Stokes + Energy + Enthalpy	–	With OpenFOAM solvers.
Solver Methodology	SIMPLE (steady), PIMPLE (unsteady)	–	Pressure-velocity coupling.

Data availability

No data was used for the research described in the article.

References

[1] G. Comodi, F. Carducci, J.Y. Sze, N. Balamurugan, A. Romagnoli, Storing energy for cooling demand management in tropical climates: a techno-economic comparison between different energy storage technologies, Energy 121 (2017) 676–694.
[2] B.K. Das, M. Hasan, Optimal sizing of a standalone hybrid system for electric and thermal loads using excess energy and waste heat, Energy 214 (2021) 119036.
[3] M.S. Ismail, M. Moghavvemi, T.M.I. Mahlia, K.M. Muttaqi, S. Moghavvemi, Effective utilization of excess energy in standalone hybrid renewable energy systems for improving comfort ability and reducing cost of energy: a review and analysis, Renew. Sust. Energ. Rev. 42 (2015) 726–734.
[4] Y.M. Han, R.Z. Wang, Y.J. Dai, Thermal stratification within the water tank, Renew. Sust. Energ. Rev. 13 (5) (2009) 1014–1026.
[5] V.V. Tyagi, D.P.C.M. Buddhi, PCM thermal storage in buildings: a state of the art, Renew. Sust. Energ. Rev. 11 (6) (2007) 1146–1166.
[6] J. Luo, D. Zou, Y. Wang, S. Wang, L. Huang, Battery thermal management systems (BTMs) based on phase change material (PCM): a comprehensive review, Chem. Eng. J. 430 (2022) 132741.
[7] P. Patel, M. Sharma, B. Mondal, H. Kothadia, Numerical study of heat transfer during solidification in ice-freezing type PCM heat exchanger, Mater. Today Proc. 47 (2021) 3288–3294.
[8] N.K. Singh, R.R. Sahoo, Hybrid thermal management system using eggshell-derived nano-enhanced multi-PCMs for hotspot mitigation in lithium-ion battery packs, Int. Commun. Heat Mass Transfer 172 (2026) 110560.
[9] A. Afzal, A. Buradi, Ü. Ağbulut, H. Bakır, M. Alwetaishi, F. Hussain, A.S. El-Shafay, S.G. Park, Unveiling the three-dimensional melting fraction of SiC nano-enhanced paraffin wax PCM in Li-ion battery pack cooling plates, Int. Commun. Heat Mass Transfer 176 (2026) 111396.
[10] S. Reddy, P. Sreedevi, A. Chamkha, Maxwell Hybrid Nanoliquid Flow over Vertical Cone with Cattaneo-Christov Heat Flux and Convective Boundary Condition, Authorea Preprints, 2020.
[11] P. Sreedevi, P.S. Reddy, Hybrid nanofluid mass and heat transport characteristics over a swirling cylinder with modified Fourier heat flux and gyrotactic microorganisms, Smart Sci. 13 (2) (2025) 121–136.
[12] P. Zuliani, F. Disegni, L. Croce, R. Annunziata, High temperature challenge for PCM as enabler for a wide spectrum of applications, in: 2019, IEEE 11th International Memory Workshop (IMW), IEEE, 2019, May, pp. 1–4.
[13] M. Pomianowski, P. Heiselberg, Y. Zhang, Review of thermal energy storage technologies based on PCM application in buildings, Energ. Buildings 67 (2013) 56–69.
[14] M. Farid, M. Smith, R. Sabbah, S. Al Hallaj, Miniaturized refrigeration system with advanced PCM micro encapsulation technology, in: International Conference on Nanochannels, Microchannels, and Minichannels 4272, 2007, January, pp. 1105–1112.
[15] C.J. Ho, J.B. Huang, P.S. Tsai, Y.M. Yang, Preparation and properties of hybrid water-based suspension of Al2O3 nanoparticles and MEPCM particles as functional forced convection fluid, Int. Commun. Heat Mass Transfer 37 (5) (2010) 490–494.
[16] T. Tayebi, A.A. Pasha, M. Danish, M.K. Al Mesfer, S. Qaiyum, M.K. Nayak, N. A. Shah, Artificial neural network prediction of an electrohydrodynamic thermosolutal buoyancy-driven convection of NEPCMs-dielectric suspension within an oblique enclosure with active blocks, Int. Commun. Heat Mass Transfer 169 (2025) 109756.
[17] P.S. Reddy, P. Sreedevi, Heat transfer investigation of thermally radiative Nano–Encapsulated Phase Change Materials (NEPCMs) in a thermal energy storage device with heat source and microorganisms, Int. Commun. Heat Mass Transfer 169 (2025) 109760.
[18] P.S. Reddy, P. Sreedevi, Impact of activation energy on heat transfer of thermally radiative nano-encapsulated phase change materials within a porous cavity with microorganisms, J. Therm. Anal. Calorim. 150 (26) (2025) 21723–21742.
[19] P.S. Reddy, P. Sreedevi, Heat and mass transport features in latent heat thermal energy storage device filled with porous media and nano-encapsulated phase change materials, J. Therm. Anal. Calorim. 150 (12) (2025) 9395–9411.
[20] A.N. Sadr, M. Shekaramiz, M. Zarinfar, A. Esmaily, H. Khoshtarash, D. Toghraie, Simulation of mixed-convection of water and nano-encapsulated phase change material inside a square cavity with a rotating hot cylinder, J. Energy Storage 47 (2022) 103606.
[21] H. Kazemi-Varnamkhasti, I. Khazaee, M. Ameri, D. Toghraie, Heat storage and increasing the rate of heat transfer in polymer electrolyte membrane fuel cell by adding nano-encapsulated phase change material to water in the cooling process, J. Energy Storage 59 (2023) 106497.
[22] C.J. Ho, Y.C. Liu, M. Ghalambaz, W.M. Yan, Forced convection heat transfer of Nano-encapsulated phase change material (NEPCM) suspension in a mini-channel heatsink, Int. J. Heat Mass Transf. 155 (2020) 119858.
[23] L. Fan, J.M. Khodadadi, A.A. Pesaran, A parametric study on thermal management of an air-cooled lithium-ion battery module for plug-in hybrid electric vehicles, J. Power Sources 238 (2013) 301–312.

[24] A.R. Bais, D.G. Subhedhar, N.C. Joshi, S. Panchal, Numerical investigation on thermal management system for lithium-ion battery using phase change material, Mater. Today Proc. 66 (2022) 1726–1733.
[25] P.M. Sutheesh, R. Thomas, R. Bandaru, Battery thermal management systems by using DI water and PCF with nano-encapsulated tetradecan-1-ol for lithium-ion batteries, Int. Commun. Heat Mass Transfer 165 (2025) 108992.
[26] J. Gu, J. Du, Y. Li, J. Li, L. Chen, Y. Chai, Y. Li, Preparation and characterization of n-octadecane@ SiO2/GO and n-octadecane@ SiO2/Ag Nanoencapsulated phase change material for immersion cooling of Li-ion battery, Energies 16 (3) (2023) 1498.
[27] A. Sarı, C. Alkan, A. Biçer, A. Altuntaş, C. Bilgin, Micro/nanoencapsulated n-nonadecane with poly (methyl methacrylate) shell for thermal energy storage, Energy Convers. Manag. 86 (2014) 614–621.
[28] M. Shekaramiz, S. Fathi, H.A. Ataabadi, H. Kazemi-Varnamkhasti, D. Toghraie, MHD nanofluid free convection inside the wavy triangular cavity considering periodic temperature boundary condition and velocity slip mechanisms, Int. J. Therm. Sci. 170 (February) (2021) 107179, https://doi.org/10.1016/j.ijthermalsci.2021.107179.
[29] B. Vahedi, E. Golab, A.N. Sadr, K. Vafai, Thermal, thermodynamic and exergoeconomic investigation of a parabolic trough collector utilizing nanofluids, Appl. Therm. Eng. 206 (2022) 118117.
[30] A.F. Turki, et al., Journal of the Taiwan institute of chemical engineers investigating the thermal performance of nano-encapsulated phase change materials-water nanofluid in the presence of a heat source as applied in electronic devices, J. Taiwan Inst. Chem. Eng. 150 (July) (2023) 105030, https://doi.org/10.1016/j.jtice.2023.105030.
[31] M.J.H. Rawa, O.S. Mahdy, N.H. Abu, Case Studies in Thermal Engineering Cooling a Cavity Equipped with a Hot Electrical Element Using Nano-Encapsulated Phase Change Material/Water: Study of Mixed Convection and Natural Convection, no. August, 2023.
[32] Omar S. Mahdy, Ali B.M. Ali, Marwah Sabah Mahdi, Dheyaa J. Jasim, Hamed Kazemi-Varnamkhasti, Mohammad Goli, Soheil Salahshour, Sh. Baghaei, Thermal performance of nanofluid natural convection magneto-hydrodynamics within a chamber equipped with a hot block, Int. J. Thermofluids 24 (2024) 100873.
[33] E. Golab, S. Goudarzi, H. Kazemi-Varnamkhasti, H. Amigh, F. Ghaemi, D. Baleanu, A. Karimipour, Investigation of the effect of adding nano-encapsulated phase change material to water in natural convection inside a rectangular cavity, J. Energy Storage 40 (2021) 102699.
[34] L. Zhang, H. Kazemi-Varnamkhasti, A. Basem, H. Hamza, A.J. Sultan, M. Al-Bahrani, C. Padilla, S.B. Formanova, S. Salahshour, A. Alizadeh, Improving the thermal performance of nano-encapsulated phase change material slurry by changing fins configurations in a rectangular cavity, Int. Commun. Heat Mass Transfer 157 (2024) 107739.
[35] X. Wang, R.H. Rasheed, B. Keivani, D.J. Jasim, A.J. Sultan, S. Hamedi, H. Kazemi-Varnamkhasti, S. Salahshour, D. Toghraie, Thermal performance of forced convection of water-NEPCM nanofluid over a semi-cylinder heat source, Case Stud. Therm. Eng. 55 (2024) 104149.
[36] Bin Guo, Ali Basem, As'ad Alizadeh, Akram Shakir Najm, Hamed Kazemi-Varnamkhasti, Dheyaa J. Jasim, Soheil Salahshour, Numerical analysis of turbulent natural convection in the presence of wire-induced non-uniform magnetic field inside a porous medium, Int. Commun. Heat Mass Transfer 160 (2025), https://doi.org/10.1016/j.icheatmasstransfer.2024.108398.
[37] E.M. Shchukina, M. Graham, Z. Zheng, D.G. Shchukin, Nanoencapsulation of phase change materials for advanced thermal energy storage systems, Chem. Soc. Rev. 47 (11) (2018) 4156–4175.
[38] S.M. Seyyedi, M. Hashemi-Tilehnoee, M. Sharifpur, Effect of inclined magnetic field on the entropy generation in an annulus filled with NEPCM suspension, Math. Probl. Eng. 2021 (2021).
[39] Z. Qiu, L. Li, Experimental and numerical investigation of laminar heat transfer of microencapsulated phase change material slurry (MPCMS) in a circular tube with constant heat flux, Sustain. Cities Soc. 52 (2020) 101786.
[40] S.Y. Motlagh, E. Golab, A.N. Sadr, Two-phase modeling of the free convection of nanofluid inside the inclined porous semi-annulus enclosure, Int. J. Mech. Sci. 164 (2019) 105183.
[41] R. Sarlak, A.M. Abed, O.A. Akbari, A. Marzban, S. Baghaei, M. Bayat, Numerical investigation of natural convection heat transfer of water/SWCNT nanofluid flow in a triangular cavity with cold fluid injection, Prog. Nucl. Energy 155 (2023) 104513.
[42] M. Ghalambaz, A.J. Chamkha, D. Wen, Natural convective flow and heat transfer of nano-encapsulated phase change materials (NEPCMs) in a cavity, Int. J. Heat Mass Transf. 138 (2019) 738–749.
[43] C.J. Ho, W.K. Liu, Y.S. Chang, C.C. Lin, Natural convection heat transfer of alumina-water nanofluid in vertical square enclosures: an experimental study, Int. J. Therm. Sci. 49 (8) (2010) 1345–1353.
[44] G.A. Sheikhzadeh, M. Dastmalchi, H. Khorasanizadeh, Effects of nanoparticles transport mechanisms on Al2O3–water nanofluid natural convection in a square enclosure, Int. J. Therm. Sci. 66 (2013) 51–62.
[45] M. Song, Y. Hu, S.Y. Choe, T.R. Garrick, Analysis of the heat generation rate of lithium-ion battery using an electrochemical thermal model, J. Electrochem. Soc. 167 (12) (2020) 120503.